Structure factor and rheology of chain molecules from molecular dynamics

Omar Castrejón-González, Jorge Castillo-Tejas, Octavio Manero, and Juan F. J. Alvarado

Citation: The Journal of Chemical Physics **138**, 184901 (2013); doi: 10.1063/1.4803526
View online: http://dx.doi.org/10.1063/1.4803526
View Table of Contents: http://scitation.aip.org/content/aip/journal/jcp/138/18?ver=pdfcov
Published by the AIP Publishing

Structure factor and rheology of chain molecules from molecular dynamics

Omar Castrejón-González,[1] Jorge Castillo-Tejas,[2] Octavio Manero,[3] and Juan F. J. Alvarado[1,a)]
[1]*Departamento de Ingeniería Química, Instituto Tecnológico de Celaya, Celaya Gto. 38010, México*
[2]*Facultad de Ciencias Básicas, Ingeniería y Tecnología, Universidad Autónoma de Tlaxcala, Apizaco Tlax. 90300, México*
[3]*Instituto de Investigaciones en Materiales, Universidad Nacional Autónoma de México, México D.F. 04510, México*

(Received 22 December 2012; accepted 17 April 2013; published online 8 May 2013)

Equilibrium and non-equilibrium molecular dynamics were performed to determine the relationship between the static structure factor, the molecular conformation, and the rheological properties of chain molecules. A spring-monomer model with Finitely Extensible Nonlinear Elastic and Lennard-Jones force field potentials was used to describe chain molecules. The equations of motion were solved for shear flow with SLLOD equations of motion integrated with Verlet's algorithm. A multiple time scale algorithm extended to non-equilibrium situations was used as the integration method. Concentric circular patterns in the structure factor were obtained, indicating an isotropic Newtonian behavior. Under simple shear flow, some peaks in the structure factor were emerged corresponding to an anisotropic pattern as chains aligned along the flow direction. Pure chain molecules and chain molecules in solution displayed shear-thinning regions. Power-law and Carreau-Yasuda models were used to adjust the generated data. Results are in qualitative agreement with rheological and light scattering experiments. © *2013 AIP Publishing LLC*. [http://dx.doi.org/10.1063/1.4803526]

INTRODUCTION

The understanding of polymer fluid dynamics is important in connection with plastics manufacture, lubrication, application of paints, processing of food, and the flow of biological fluids.[1] Flow behavior of viscoelastic fluids, such as polymer solutions, is more complex than that of the familiar Newtonian fluids. These fluids display shear thinning, normal-stresses, shear thickening, die swell, memory effects, etc. These effects are strongly correlated with flow-induced conformational changes of the polymer chains and these changes are often dramatic. The orientation and deformation of polymers due to flow have been measured by flow birefringence, light scattering, and neutron scattering experiments, but they may also be studied by computer simulations.

A semi-dilute polymer solution in a single phase may exhibit strong turbidity when subjected to shear flow due to shear-induced enhancement of concentration fluctuations and/or phase separation. This phenomenon is one of the most remarkable properties of these solutions and it is attributed to dynamical coupling between stress and diffusion. The local variation of the composition influences the local stress. Under shear flow, the local stress increases in the region having large polymer concentration.[2]

Experimentally, the enhancement of concentration fluctuations due to flow has been observed by light scattering (LS) and small angle neutron scattering (SANS). In several reports, the static structure factor was determined for a semi-dilute solution of polystyrene in di-octyl-phthalate (PS/DOP) in shear[3–6] and extensional[7] flows. The evolution of the structure factor in the flow field was visualized as a series of contour plots. The scattering pattern becomes anisotropic due to chains alignment induced by flow.

Milner[8] proposed a model to calculate the structure factor coupled with rheological constitutive equations. In this model both the amplitude of the concentration fluctuations and the viscoelastic responses were linearized with respect to the concentration fluctuations and the shear rate. The shape of these structure factors was found to agree, qualitatively, with the observed scattering intensity distribution, indeed demonstrating that the theory describes the enhancement of concentration fluctuations under shear flow. However, most calculations of the structure factor and the comparisons with experimental results have been limited to the shear rate region satisfying **We** $\leq$1.0 where **We** is the Weissenberg number.[2]

Rheology provides an indirect, and hence limited, indicator of material structure at molecular level. Rheological measurements are more useful when combined with direct ways of elucidate the structure of the material under flow, such as microscopy, birefringence, light scattering, polarimetry, among others.[9] The orientation and deformation of chain molecules have been measured, for example, using flow birefringence, light scattering, and neutron scattering experiments. Computer simulation methods have complemented such experimental techniques.[10–15]

Molecular dynamics (MD) simulations, on the other hand, provide a powerful tool to investigate the microscopic underlying mechanisms of macroscopically observable transport phenomena.[16] The main advantage of simulation techniques over other methods is the possibility to calculate physical properties of systems at conditions that are difficult

a)Author to whom correspondence should be addressed. Electronic mail: javier@iqcelaya.itc.mx

to approach experimentally.[17] Several equilibrium MD procedures have been developed[18–20] to compute the static structure factor with one-dimensional wave vectors analyzing the effect of the chain molecules. Recently, MD has been used also as a complement to experimental studies. Such is the case of Burchard *et al.*[21] who employed static and dynamic light scattering, combined along with equilibrium MD to characterize experimental results of hyper-branched polymers.

Laun *et al.*[22] reported one early work where SANS scattering patterns were compared to Non-Equilibrium Molecular Dynamics (NEMD) simulations. They conducted rheological studies of concentrated polymer dispersions (styrene-ethylacrylate-copolymer spheres in glycol or water) by SANS in a wide range of shear rates. Their results showed regions of shear thinning and shear thickening as functions of the applied shear rates. The obtained SANS scattering patterns were compared to NEMD simulations employing soft sphere models. In spite of the simple particle model used, the scattering patterns obtained from simulation exhibited a remarkable similarity to the directly measured SANS data. Aust *et al.*,[23] used NEMD to study systems of Finitely Extensible Nonlinear Elastic (FENE) + Weeks-Chandler-Andersen (WCA) chains with various lengths in dilute solutions at good solvent conditions. They concluded that, regarding rheology, there is an effect of chain length on the shear viscosity for the intrinsic viscosity extracted from the intramolecular interactions. The normal stresses produced by the solvent were negligibly small compared to those calculated for the model polymer solution. A particular result that we observed also in our calculations is that the solvent, modeled as purely repulsive Lennard-Jones (LJ) potential (WCA), exhibited non-Newtonian behavior at shear rates above 0.3 ($\dot{\gamma} > 0.3$).

Jose and Szamel[24] reported recently a Brownian dynamics computer simulation study on the structural properties of semidilute polymer solutions in shear flow. The polymer model was a truncated and shifted Lennard-Jones potential with FENE potential used for the bond connectivity. Chains of 10 monomers were used in the calculations which were conducted at reduced temperature of $k_BT/\epsilon = 4.0$. The main finding, as reported by these authors, was that the anisotropic deformation of the solution structure factor could be reproduced using a simple model system which included relatively short chains and overdamped Brownian dynamics without any hydrodynamic interactions. The structure factors reproduced the experimentally observed butterfly patterns by Wu *et al.*[3]

For the last four decades Molecular Dynamics studies have offered a wide understanding about the dynamics of polymers. The reason for this is due to the natural way that MD links the conformational properties of polymers with their macroscopic properties. In this work extensive NEMD studies of a simple shear flow of chain molecules are performed. The main objective of this NEMD study is to elucidate, at the molecular level, the relationship between rheological properties, static structure factors, and molecular conformation of chain molecules in solution. As far as we know, this study reports for the first time results for chain solutions in good solvent condition at three different concentrations; range from semi-dilute solution to pure chains (melt). We employ commonly used dispersive force fields to model the particle interactions. The study provides, in this manner, detailed information about changes in the rheology of polymer solutions.

METHODOLOGY

Model and simulation

Flexible linear chains in good solvent conditions were simulated. Both, the solvent and the chain molecules were built of spherical particles of equal mass m and diameter σ. The truncated and shifted Lennard-Jones potential was used to model pair interactions between non-bonded particles which include: solvent-solvent, solvent-bead, and non-bonded beads interactions

$$U_{ij}^{\mathrm{LJ}} = \begin{cases} 4\epsilon\left[\left(\frac{\sigma}{r_{ij}}\right)^{12} - \left(\frac{\sigma}{r_{ij}}\right)^{6}\right] + \epsilon, & r_{ij} \le r_c \\ 0, & r_{ij} > r_c, \end{cases} \quad (1)$$

the cut-off ratio for the solvent-solvent interaction was fixed to $r_c = 2.5\sigma$, meanwhile for the solvent-bead and non-bonded beads it was $r_c = 2^{1/2}\sigma$ (WCA potential). The potential between chain-bonded segments is modeled by the sum of two terms: the first one is the FENE attractive potential which extends to the maximum bond extension R_0.[25] The second term is the LJ potential at a cut-off ratio of $2^{1/6}\sigma$; the locus of the minimum in the LJ potential function. This potential is implemented in LAMMPS (Large-scale Atomic/Molecular Massively Parallel Simulator)[26] for bead spring chains:

$$U_{ij}^{b} = -0.5\,k_f\,R_0^2 \ln\left[1 - \left(\frac{r_{ij}}{R_0}\right)^2\right] + 4\epsilon\left[\left(\frac{\sigma}{r_{ij}}\right)^{12} - \left(\frac{\sigma}{r_{ij}}\right)^{6}\right] + \epsilon, \quad (2)$$

where k_f is a sort of spring constant. Figure 1 summarizes the particle interactions.

NEMD simulations in the NVT ensemble were performed using the SLLOD equations of motion for a homogeneous shear flow,[27] which is equivalent to the p-SLLOD equations for planar Couette flow.[15] The Nosè-Hoover thermostat[28,29] was applied to keep the temperature constant.

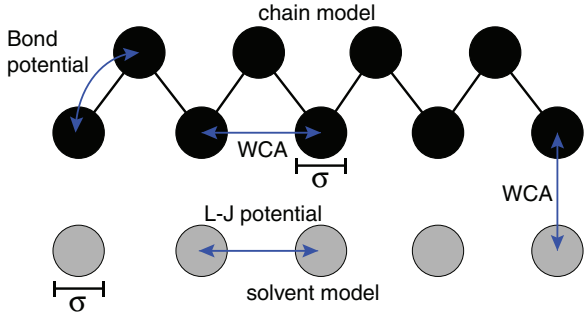

FIG. 1. Particle interactions scheme. Dark circles correspond to beads in the chain molecules. Light circles represent solvent particles. Non-bonded particles, including solvent and beads, interact with truncated and shifted Lennard-Jones potential while bonded chains are represented by a FENE + Lennard-Jones potential.

The equations of motion are:

$$\dot{\boldsymbol{q}}_{ia} = \frac{\boldsymbol{p}_{ia}}{m_{ia}} + \boldsymbol{q}_{ia}\cdot\nabla\boldsymbol{v}, \tag{3}$$

$$\dot{\boldsymbol{p}}_{ia} = \boldsymbol{F}_{ia} - \boldsymbol{p}_{ia}\cdot\nabla\boldsymbol{v} - \varsigma\,\boldsymbol{p}_{ia}, \tag{4}$$

$$\dot{\varsigma} = \frac{p_\varsigma}{Q}, \quad Q = 3Nk_BT\,\tau^2, \tag{5}$$

$$\dot{p}_\varsigma = \sum_i \sum_a \frac{p_{ia}^2}{m_{ia}} - 3Nk_BT, \tag{6}$$

where subscripts i and a are used to distinguish molecules from particles, respectively, and the dot notation means time derivative. The symbols $\boldsymbol{q}_{ia}$, $\boldsymbol{p}_{ia}$, $\boldsymbol{F}_{ia}$, and m_{ia} represent the position, momentum, and force vectors, and the mass of particle a in molecule i, respectively. N is the total number of particles, T is the temperature, and k_B is the Boltzmann constant. Q, ς, p_ς, and τ represent the inertial mass, coordinates, momenta, and dimensionless time, respectively, of the Nosè-Hoover thermostat. The velocity gradient tensor $\nabla\boldsymbol{v}$ in shear flow is given by

$$\nabla\boldsymbol{v} = \begin{bmatrix} 0 & 0 & 0 \\ \dot{\gamma} & 0 & 0 \\ 0 & 0 & 0 \end{bmatrix}, \tag{7}$$

where $\dot{\gamma}$ is the applied shear rate.

The whole set of variables is in reduced units; the relevant parameters are: $\rho^* = \rho\sigma^3$, $T^* = k_BT/\epsilon$, $U^* = U/\epsilon$, $\boldsymbol{P}^* = \boldsymbol{P}\sigma^3/\epsilon$, $t^* = t(\epsilon/\sigma^2 m)^{1/2}$, $\dot{\gamma}^* = \dot{\gamma}(m/\sigma^2\epsilon)^{1/2}$, and $\eta^* = \eta\sigma^2/(m\epsilon)^{-1/2}$, where ρ is the local density, U is the energy, $\boldsymbol{P}$ is the pressure tensor, η is the viscosity, and t is the time. For simplicity, hereafter the asterisk notation will be omitted.

Regarding the temperature, MacDowell *et al.*[30] calculated, using Monte Carlo simulation, the critical temperature of chain molecules of various lengths. Using truncated and shifted Lennard-Jones and FENE potentials to model particle interactions, similar to those employed in this work, they found that for infinite length chains, the critical temperature asymptotically reaches a value of $3.3\epsilon/k_B$. According to this report we felt appropriate to take a reduced temperature of $k_bT/\epsilon = 4.0$ in our calculations. In this manner we ensure that our systems were in liquid state. Furthermore, Heyes[31] reported that for a Lennard-Jones fluid, the solvent in our case, its shear viscosity remains constant at this reduced temperature for a wide range of shear rate. The rest of the parameters used in the simulation are shown in Table I.

TABLE I. Dimensionless variables and parameters used in simulation.

Variable	Symbol	Value
Particle mass	m	1.0
Particle diameter	σ	1.0
Energy	ϵ	1.0
Density	ρ	0.84
Temperature	T	4.0
FENE's constant	k_v	30
Maximum bond length	R_0	1.5

Structure factor

The structure factor $S(\boldsymbol{k})$ is defined as the autocorrelation function:[32]

$$S(\boldsymbol{k}) = \frac{1}{N}\langle\rho_{\boldsymbol{k}}\rho_{-\boldsymbol{k}}\rangle, \tag{8}$$

where

$$\rho_{\boldsymbol{k}} = \sum_{j=1}^{N} \exp(-i\boldsymbol{k}\cdot\boldsymbol{r}_j) \tag{9}$$

is the Fourier transform of the microscopic (total) density and $\boldsymbol{r}_j$ denotes the position of particle j, with $1 \le j \le N$. This equation, together with the Euler's identity: $\exp(\pm ia) = \cos(a) \pm i\sin(a)$ allows computing static structure factors from molecular simulation. The minimum $\boldsymbol{k}$ vector for a box of length L for the N particle system is[33] $(2\pi/L)$ and hence, the components of the $\boldsymbol{k}$ vector are restricted, due to periodic boundary conditions, to multiples of $(2\pi/L)$. If $\boldsymbol{k}$ has only components x and y, then:

$$\boldsymbol{k} = k_x\hat{\boldsymbol{x}} + k_y\hat{\boldsymbol{y}} = n_x\left(\frac{2\pi}{L}\right)\hat{\boldsymbol{x}} + n_y\left(\frac{2\pi}{L}\right)\hat{\boldsymbol{y}}, \tag{10}$$

where n_x and n_y are integer numbers.

The structure factor can be measured directly through radiation scattering experiments; in particular, from Static Light Scattering (SLS). This experimental technique has been a useful tool to elucidate the molecular structure of materials. It has been used to determine density fluctuations of a system due to external light perturbation with a wavelength of $2\pi/k$. In particular, the SLS has been widely used to characterize polymer chains in solution. The weight-average molecular weight M_w, the radius of gyration R_g, and the second virial coefficient B_2 are some of polymer properties that can be obtained from SLS experiments.

In a dilute polymeric solution formed by n_p chains $(n_p \gg 1)$, with N monomers per chain, the static structure factor, also called scattering function, for a single chain can be obtained from[34]

$$S_1(\boldsymbol{k}) = \frac{1}{N}\sum_{j,k=1}^{N}\langle\exp[i\boldsymbol{k}\cdot(\boldsymbol{r}_i - \boldsymbol{r}_j)]\rangle, \tag{11}$$

where $\boldsymbol{k}$ is the scattering vector which is the difference between the scattered beam wave vector $\boldsymbol{k}_s$ and the incident beam wave vector $\boldsymbol{k}_o$. For finite concentrations, the interference between monomers of neighbor chains must be taken into account. In this case, the structure factor is given by

$$S(\boldsymbol{k}) = S_1(\boldsymbol{k}) + \frac{n_p}{N}\sum_{i,j=1}^{N}\langle\exp[i\boldsymbol{k}\cdot(\boldsymbol{r}_{1i} - \boldsymbol{r}_{2j})]\rangle, \tag{12}$$

the second term adds up the correlations between nearby chains 1 and 2. At low concentrations, however, the statistical average for different chains is mostly zero, and $S(\boldsymbol{k})$ becomes identical to $S_1(\boldsymbol{k})$.

Rheological models

Considerations are here given to describe the shear behavior of the non-Newtonian polymer solutions. The shear-thinning region of polymer solutions is usually modeled by a power-law equation (also called Ostwald de Waele model),

$$\boldsymbol{\tau} = K\dot{\gamma}^n, \tag{13}$$

where K is the consistency index and n is called the flow index. The Carreau-Yasuda[35,36] equation, on the other hand, has proved to be an excellent model to fit the whole shear rate interval, including the Newtonian and the shear-thinning regions. The equation is given by

$$\eta = \frac{\eta_0}{[1+(\lambda\dot{\gamma})^2]^p}, \tag{14}$$

where η_0 is the zero shear rate viscosity, λ is a characteristic time constant, $\dot{\gamma}$ is the shear rate, and p is a numerical exponent.

Material functions

The pressure tensor $\boldsymbol{P}$ is given by a sum of site-site contributions:

$$P_{kl} = -\frac{1}{V}\left[\sum_i \frac{p_{ki}p_{li}}{m_i} + \frac{1}{2}\sum_i\sum_{j>i} r_{kij}F_{lij}\right], \tag{15}$$

where P_{kl} is the pressure tensor component acting along l direction through a normal plane to the k axis, p_{ki} and p_{li} are the k and l components of the momentum of particle i and m_i its associated mass. Furthermore, V is the system volume, r_{kij} is the k-component of the scalar distance r_{ij}, and F_{lij} is the l-component of the force resulting from the interaction between particles i and j. The first term of Eq. (15) represents the kinetic contribution and the second arises from pair interactions (LJ and FENE potentials). For the system studied here, the main contribution to pressure tensor stems from the pair potentials.

The viscometric functions, namely the shear viscosity η, and the first and second normal stress coefficients are defined by

$$\eta = -\frac{P_{xy}}{\dot{\gamma}}, \tag{16}$$

$$\Psi_1 = \frac{P_{xx}-P_{yy}}{\dot{\gamma}^2} = \frac{N_1}{\dot{\gamma}^2}, \tag{17}$$

$$\Psi_2 = \frac{P_{yy}-P_{zz}}{\dot{\gamma}^2} = \frac{N_2}{\dot{\gamma}^2}. \tag{18}$$

RESULTS AND DISCUSSION

The system used in the simulations consisted in 60 chains N_{ch} with a length N_b of 100 beads each. The chains are immersed in a bath of N_s solvent particles. Calculations were performed for 0.0 (pure solvent), 0.1, 0.5, and 1.0 chain mass fractions. The mass fraction ϕ was calculated as

$$\phi = \frac{N_{ch}N_b}{N_{ch}N_b + N_s}. \tag{19}$$

Accordingly this, the solutions will be identified, hereafter as the 0.0, 0.1, 0.5, and 1.0 solutions.

Equilibrium molecular dynamics

At equilibrium conditions ($\dot{\gamma} = 0$) the final configurations show a random distribution of particles, indicating an isotropic state. In Figure 2 we observe the corresponding projections of the static structure factor in two dimensions. Concentric circular shapes in the structure factor plots show evidence of an isotropic distribution of particles; the structure factor as a function of scattering vector is independent of the measuring direction. Observing the shape of the scattering patterns, results obtained from these simulations and light scattering experiments[5] are in qualitative agreement.

Non-equilibrium molecular dynamics

Non-equilibrium molecular dynamics simulation under simple shear Couette flow was performed. The flow was in the x direction, the velocity gradient in the y direction, meanwhile the vorticity was along the z direction. The whole set of simulations was performed using the LAMMPS[26] code where a triclinic box was used to enclose the particles. A total of 6×10^6 time steps were performed for each simulation run with a time step length of 0.005. The initial 2×10^5 integration steps were performed for equilibration purposes. A shear strain was applied to the simulation space causing the deformation of the box. The amount of tilt or skew that can be applied to the simulation box was limited (for computational efficiency) to be one half of the parallel box length. The strain, however, can deform the box continuously by any arbitrary amount. When the tilt reaches the limit, the box was re-shaped to the opposite limit; this is an equivalent tilting of periodic space. In a long NEMD simulation these box reshaping events may occur many times.

Rheological characterization

Prior to the NEMD simulations, the radial distribution function was calculated to ensure that the simulated system was initially in liquid state. The calculated shear viscosity as a function of the shear rate is depicted in Figure 3. There, two regions can be distinguished: a Newtonian region at low shear rates and a shear thinning region from intermediate to high shear rates. The smallest viscosities correspond to the pure solvent and increase with the chain concentration. The solvent, which is modeled as a LJ fluid, displays a closely constant viscosity for the whole range of shear rates, indicating a Newtonian behavior.

Parameters of the Power-law model (13), used to adjust the simulation data are depicted in Table II. The adjustment of data in the shear thinning region with the Power-law model is quite good for the pure chains meanwhile the pure

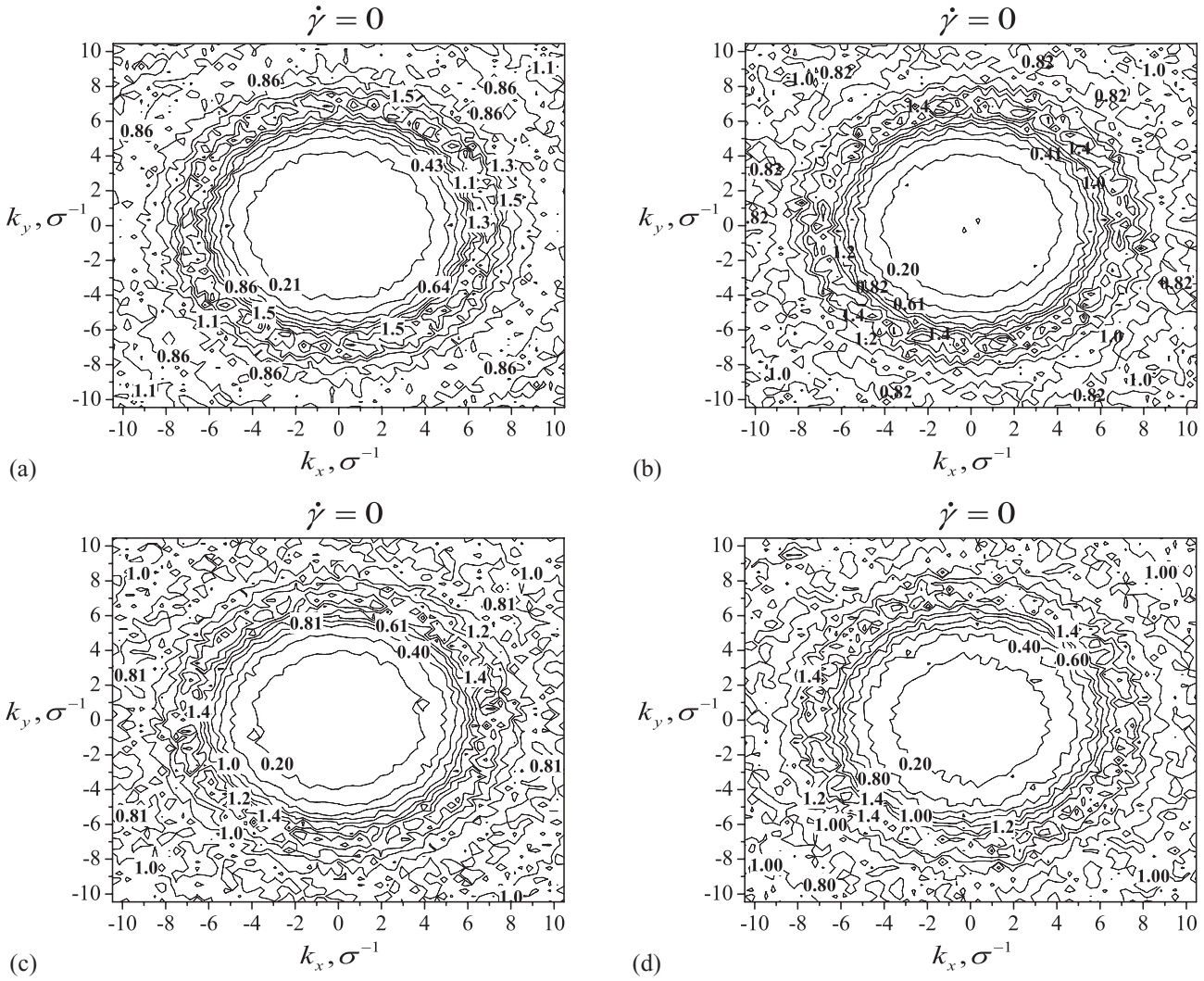

FIG. 2. Structure factor projections on the x-y plane at $\dot{\gamma} = 0$. There is isotropy in all cases: (a) 0.0, (b) 0.1, (c) 0.5, and (d) 1.0 solutions.

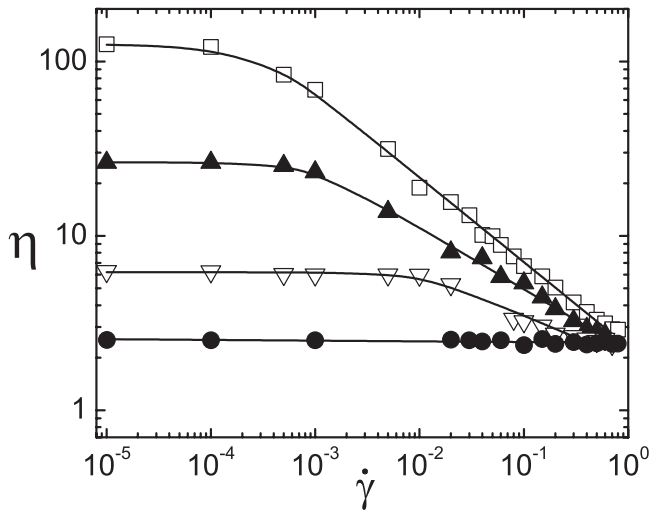

FIG. 3. Shear viscosity vs. shear rate for the 0.0 (●), 0.1 (▽), 0.5 (▲), and 1.0 (□) solutions. Power law model fits well the simulated data in the shear thinning region, while the Carreau-Yasuda model fits the behavior of simulated data in the whole range of shear rates.

solvent behaves closely as a Newtonian fluid. The smallest Power-law index n corresponds to the pure chains ($n = 0.4958$). It increases as the chain concentration decreases until $n \approx 1.0$ for the solvent. Good qualitative agreement with experimental data[37] is obtained.

Table II contains also the parameters of the Carreau-Yasuda model (14) obtained in the adjustment of the simulated data in the whole shear rate range. The p parameter shows a tendency to increase with the chain concentration. The time constant λ is the inverse of the strain rate at the

TABLE II. Parameters of Power-Law and Carreau-Yasuda models that fit simulation data.

ϕ	K	n	η_0	λ	p
0.00	2.4348	0.9948	2.57		
0.10	1.9924	0.7624	6.18	97	0.126
0.50	3.2020	0.7619	26.41	1132	0.177
1.00	2.1110	0.4958	124.52	3669	0.243

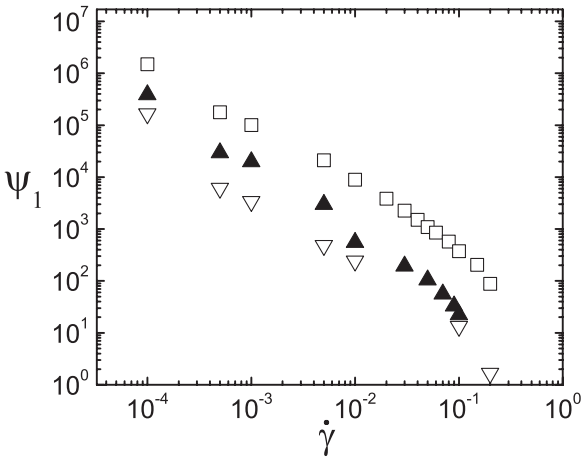

FIG. 4. First normal stress coefficient vs. shear rate for the 0.1 (▽), 0.5 (▲), and 1.0 (□) solutions.

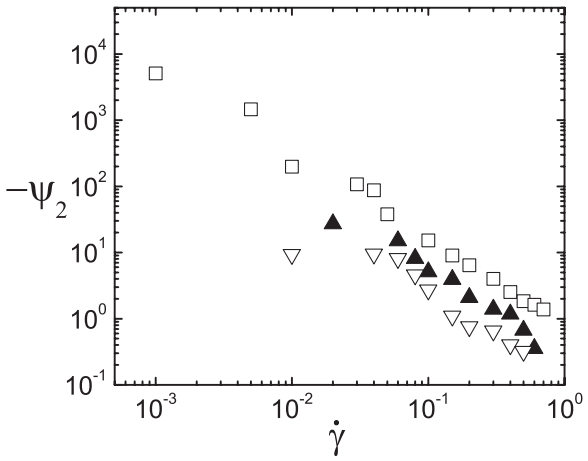

FIG. 5. Second normal stress coefficient vs. shear rate for 0.1 (▽), 0.5 (▲), and 1.0 (□) solutions.

onset of the shear-thinning region.[10] In this way, the inverse of λ marks the shear rate at which the transition between the Newtonian plateau and the shear thinning region occurs. The inverse of λ for the 0.1, 0.5, and 1.0 solutions are, approximately, 0.01, 0.0009, and 0.0003, respectively. These values are consistent with the shear viscosity behavior obtained from the shear viscosity curve displayed in Figure 3.

The first and second normal stress coefficients are plotted in Figures 4 and 5, respectively. Consistent with existing experimental results, these coefficients show an increasing shear-thinning behavior with the shear rate. Also, at equal shear rate, the normal stress coefficients are larger for solutions with larger chain concentration. This behavior indicates that the chain molecules enhance the elasticity of solutions. Data for the first normal stress coefficient were fitted with a power law model: $\psi_1 = M\dot{\gamma}^{-\alpha}$. The parameter M follows a pronounced increase with the chain concentration; being 0.002, 0.335, and 12.136 for the 0.1, 0.5, and 1.0 solutions, respectively. Parameters α which takes the values 1.973, 1.515, and 1.273 for the 0.1, 0.5, and 1.0 solutions, respectively, are very close to the values obtained for similar NEMD simulation results by Le *et al.*[12] and Bosko *et al.*[38] These values are within the range of experimental values for pure polymers and concentrated solutions.[1] In order to assess our results in the context of the literature, Table III displays some rheological parameters calculated in this work and compare them with those reported from other sources. As may be seen, our results fit quite well with this previous work.

The second normal stress coefficient has been studied less extensively in experiments than the first coefficient. It is negative and smaller in magnitude than the first normal stress coefficient.[13] In Figure 6, the ratio of the second and first normal stress coefficients vs. shear rate for the pure chains is depicted. For linear polymers this ratio is between 0.05 and 0.15.[38] Calculated results show an agreement with experimental data for typical polymers.[1]

The absolute value of the first normal stress difference ($N_1 = P_{xx} - P_{yy}$) as a function of the shear rate is presented in Figure 7 illustrating agreement with experimental data reported by Kontopoulou[40] for polymer solutions and Kulicke and Wallbaum[41] for polystyrene in toluene. For the pure solvent—a Lennard-Jones fluid—the curve behavior, however, is not consistent with that of a Newtonian fluid for which N_1 must be zero. The simulated results suggest that the LJ fluid is not wholly representative of the reference Newtonian behavior. This behavior was also found by Castillo-Tejas *et al.*,[42] Heyes,[43] and Aust *et al.*[23]

Structure of the Lennard-Jones solvent

Although the Lennard-Jones fluid exhibits an approximately constant viscosity in the whole shear viscosity range, a small value different from zero in the first normal stress difference is observed. However, the absence of molecular ordering (isotropy) in the solvent is confirmed by showing its structure factor patterns. The results are depicted in Figure 8. There,

TABLE III. Comparative table of some rheological parameters.

Author	N_b (Beads)	$[\eta \propto \dot{\gamma}^{-m}]$ m	$[\psi_1 \propto \dot{\gamma}^{-\alpha}]$ α	$[\psi_2 \propto \dot{\gamma}^{-\beta}]$ β	$(-N_2/N_1)$ range
This work	100	0.5	1.27	1.29	0.02–0.12
Daivis *et al.*[11]	50	0.45	1.35	1.36	NA
Kröger *et al.*[16]	100	0.47	1.5	NA	0.01–0.26
Aust *et al.*[23]	60	0.59	1.15	NA	NA
Bosko *et al.*[38]	91	0.523	1.306	1.537	0.05–0.15
Chen *et al.*[39]	100	0.56	NA	NA	0.1–0.2

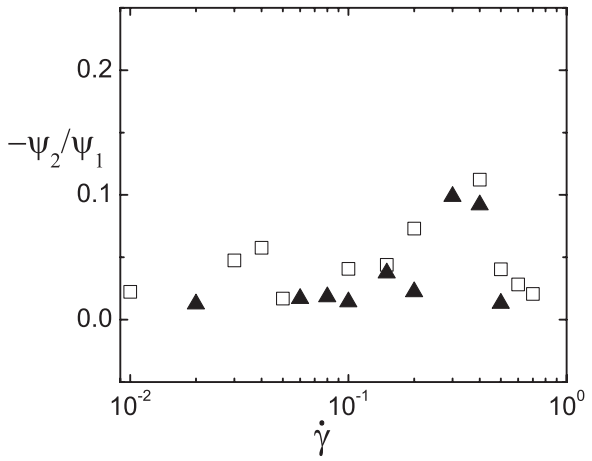

FIG. 6. Ratios of the second and first normal stress coefficients vs. shear rate for the 0.5 (▲) and 1.0 (□) solutions.

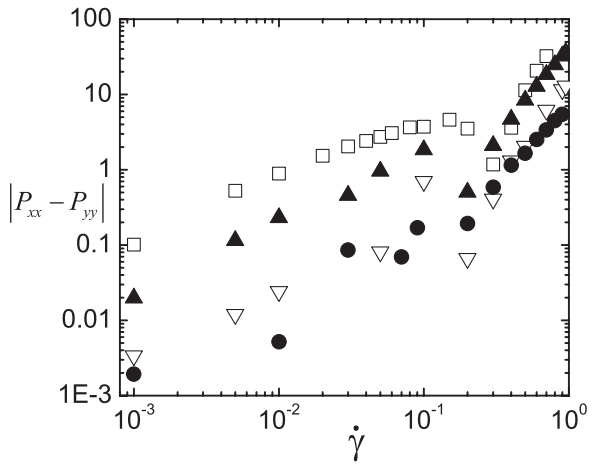

FIG. 7. Absolute value of the first normal stress difference vs. shear rate for the 0.0 (●), 0.1 (▽), 0.5 (▲), and 1.0 (□) solutions.

the structure factor shows concentric-circle patterns for both low and high shear rates, which is indicative that flow does not induce ordering on the solvent.

Structure of the chain molecules in solution

Figures 9 and 10 display the structure factor patterns developed by the chain molecules for the 0.1 and 0.5 solutions, respectively, and at two shear rates. The contribution of the solvent to the structure factor has been omitted, and only the coordinates of the chain molecules are considered for this quantity. In both figures there are marked differences of the structure factor patterns at the two shear rates. At the low shear rate of 0.01 both patterns display two large peaks close to the center (small scattering vector $\boldsymbol{k}$) with maxima of $S(k_x, k_y) = 4.84$ for the 0.1 solution and $S(k_x, k_y) = 4.54$ for the 0.5 solution. For large scattering vectors, the structure factors display a concentric circular pattern. The 0.5 solution displays even a full symmetry in all radial directions. This concentric circular pattern and symmetry indicates that, at low shear rates, the chain molecules in the solutions are randomly arranged in an isotropic state. On the other hand, for the high shear rate of 0.7, the peaks are displaced away from the center and aligned in the flow direction. This alignment reveals that the chains are also aligned in that direction. There are two symmetric regions of peaks with maxima of $S(k_x, k_y) = 4.82$ for the 0.1 solution and $S(k_x, k_y) = 3.41$ for the 0.5 solution. The axis of symmetry, in both cases, is slightly tilted with respect to the horizontal. There are also, along the vertical direction, two incipient peaks located in the extremes with maxima of $S(k_x, k_y) = 3.012$ for the 0.1 solution and $S(k_x, k_y) = 2.131$ for the 0.5 solution. Figure 11 depicts results for pure chains. At the low shear rate of 0.01, the structure factor displays concentric circles pattern which indicates an isotropic state for the chain molecules. At the high shear rate of 0.7, there are six regions in the structure factor pattern with large and well defined peaks. One of these regions corresponds to the peaks located along the vertical axis of the dispersion pattern. The static structure factor for the six peaks reaches now a maximum of $S(k_x, k_y) = 2.9$. This pattern resembles the

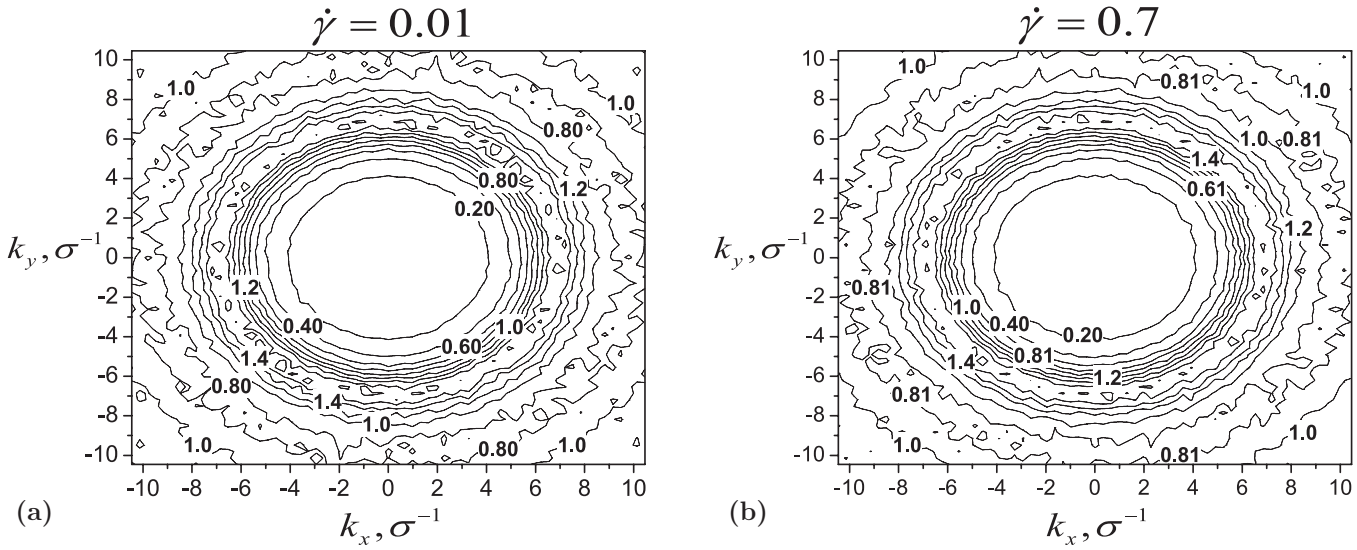

FIG. 8. Structure factor patterns on the *x*-*y* plane of the pure solvent at shear rates of (a) $\dot{\gamma} = 0.1$ and (b) $\dot{\gamma} = 0.7$. Both cases display isotropic behavior.

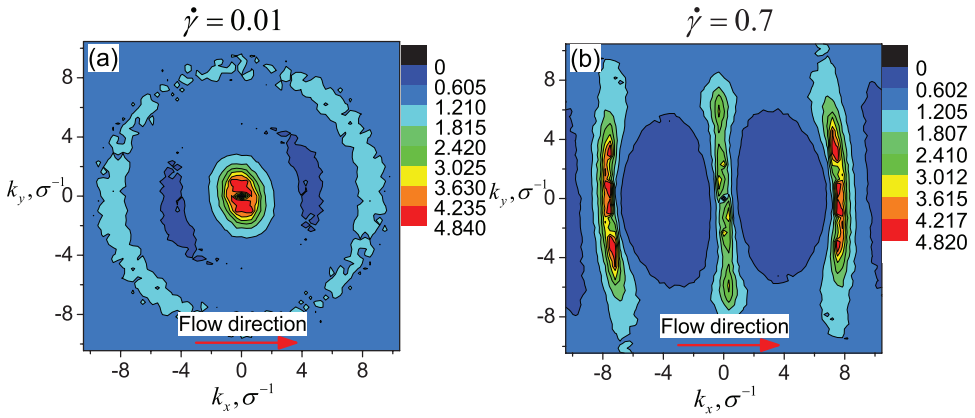

FIG. 9. Structure factor patterns on the *x*-*y* plane of the 0.1 solution at shear rates of (a) $\dot{\gamma} = 0.01$ and (b) $\dot{\gamma} = 0.7$.

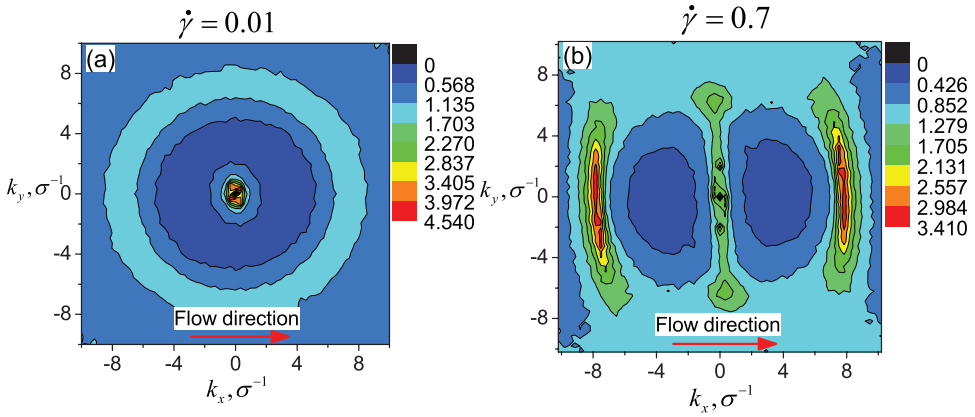

FIG. 10. Structure factor patterns on the *x*-*y* plane of the 0.5 solution at shear rates of (a) $\dot{\gamma} = 0.01$ and (b) $\dot{\gamma} = 0.7$.

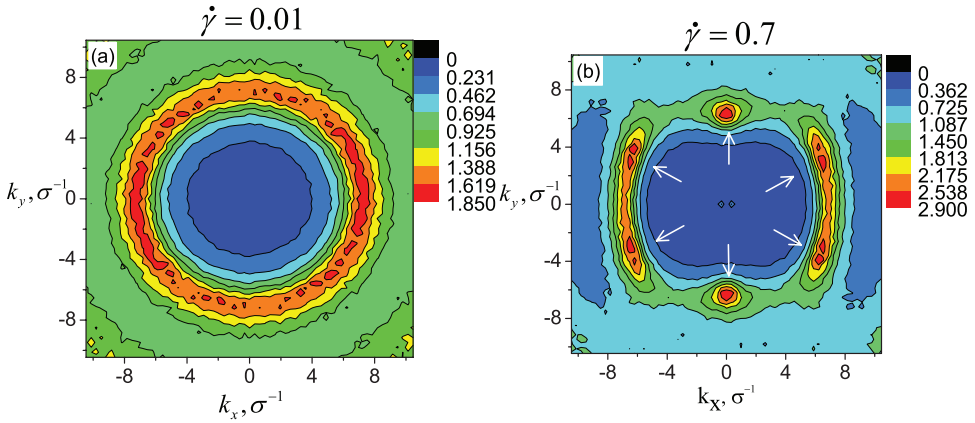

FIG. 11. Structure factor patterns on the *x*-*y* plane of pure chains at shear rates of (a) $\dot{\gamma} = 0.01$ and (b) $\dot{\gamma} = 0.7$.

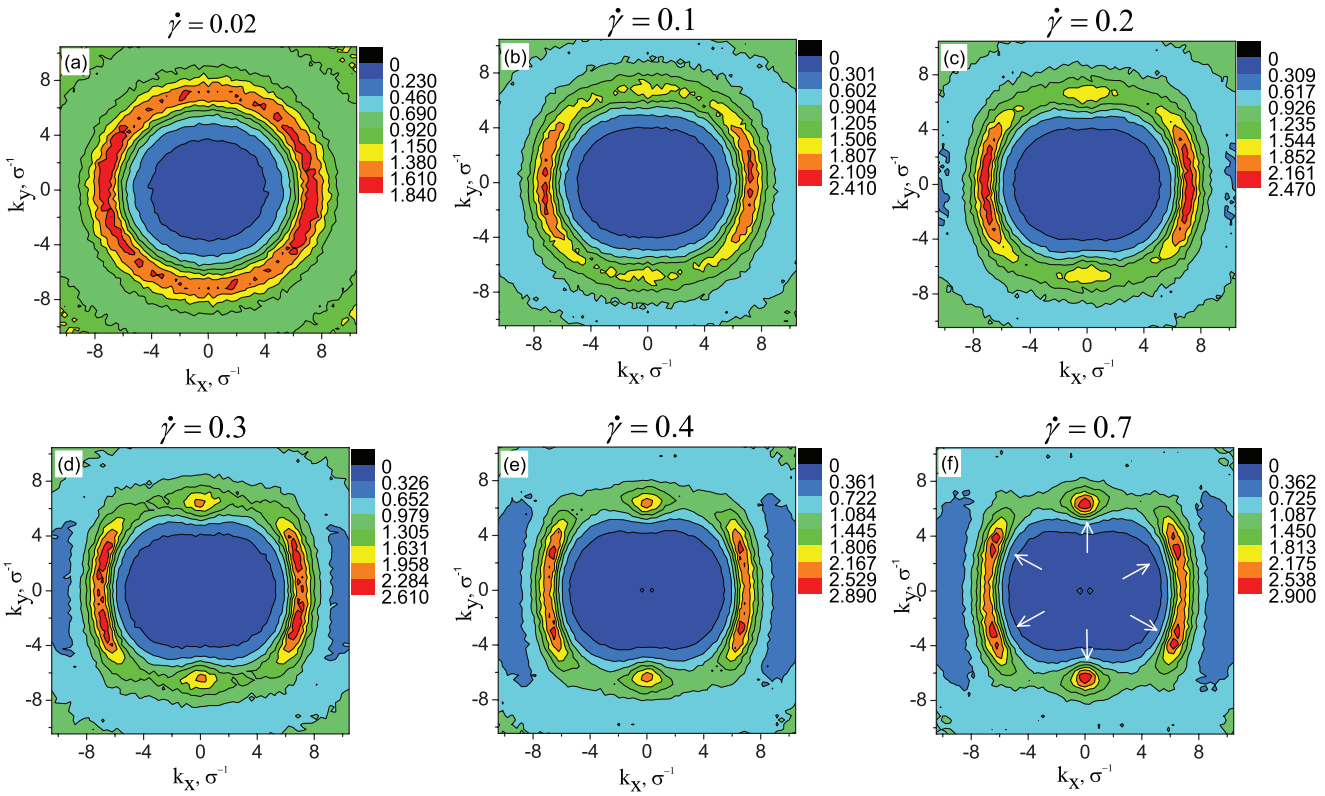

FIG. 12. Evolution of the structure factor patterns on the *x*-*y* plane as a function of the shear rate at the shear-thinning region for the pure chain molecules. (a) $\dot{\gamma} = 0.02$, (b) $\dot{\gamma} = 0.1$, (c) $\dot{\gamma} = 0.2$, (d) $\dot{\gamma} = 0.3$, (e) $\dot{\gamma} = 0.4$, and (f) $\dot{\gamma} = 0.7$. Peaks appear as the shear rate increases. The scattering pattern changes are due to molecular organization.

experimental SANS intensity patterns reported by Laun *et al.*[22] for styrene-ethylacrylate copolymer dispersions in glycol and water.

Chain alignment along the flow direction for a shear rate of $\dot{\gamma} = 0.7$ can be deduced from Figures 9–11. An increase in the number of peaks on the structure factor is observed with well-defined peaks, as the chain concentration increases in the solution, due to an increase of the dispersed light. The shape of the central blue region in the structure factor projection evolves as a function of the shear rate; from an ellipsoidal shape for isotropic solutions—at low shear rate—to overlapped circles for non-isotropic solutions—at high shear rate—when the chains align in the flow direction. The presence of new peaks in the structure factor is due to the augmented dispersion as the concentration and orientation of the chains increase. On the other hand, the intensity of dispersion, which can be related directly with the magnitude of the structure factor at the peaks, decreases with the chain concentration. For example, for the solution at a shear rate of 0.7 the maxima of $S(k_x, k_y)$ are 4.82, 3.41, and 2.9 for the chain mass fractions of 0.1, 0.5, and 1.0, respectively.

Evolution of the static structure factor

Static structure factors were computed with code developed based upon the Rapaport's codes[44] and the molecular conformation snapshots employed the Visual Molecular Dynamics (VMD)[45] and Ovito[46] softwares.

In Figure 12, the evolution of $S(\boldsymbol{k})$ as a function of shear rate is displayed. Two new peaks emerge, corresponding to the change in the radius of gyration of the chain molecules when they align, as it is shown in Figure 13. The magnitude of the peaks increases in proportion to the shear rate.

Deformation in the structure factor pattern is due to the anisotropy of the solution induced by the flow. As the chains align with the flow, six peaks in the scattering pattern emerge, whose magnitude depends on the shear rate. Figure 14 displays the relation between structure, viscosity, and molecular

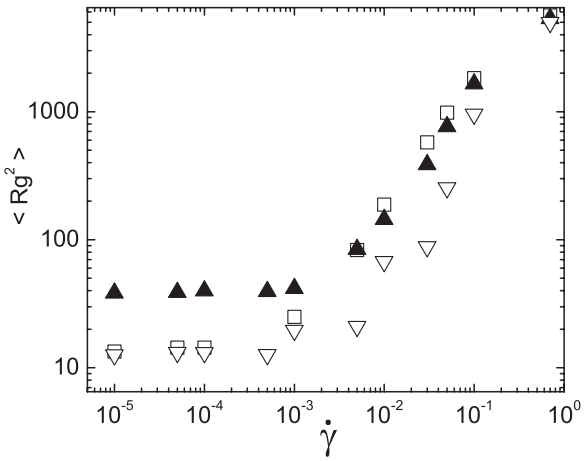

FIG. 13. Mean square radius of gyration as a function of shear rate. The increasing in the value of this parameter with the shear rate evidences the alignment of the chains along the flow. Symbols differentiate chain mass fraction in the solution: 0.1 (▽), 0.5 (▲), and 1.0 (□).

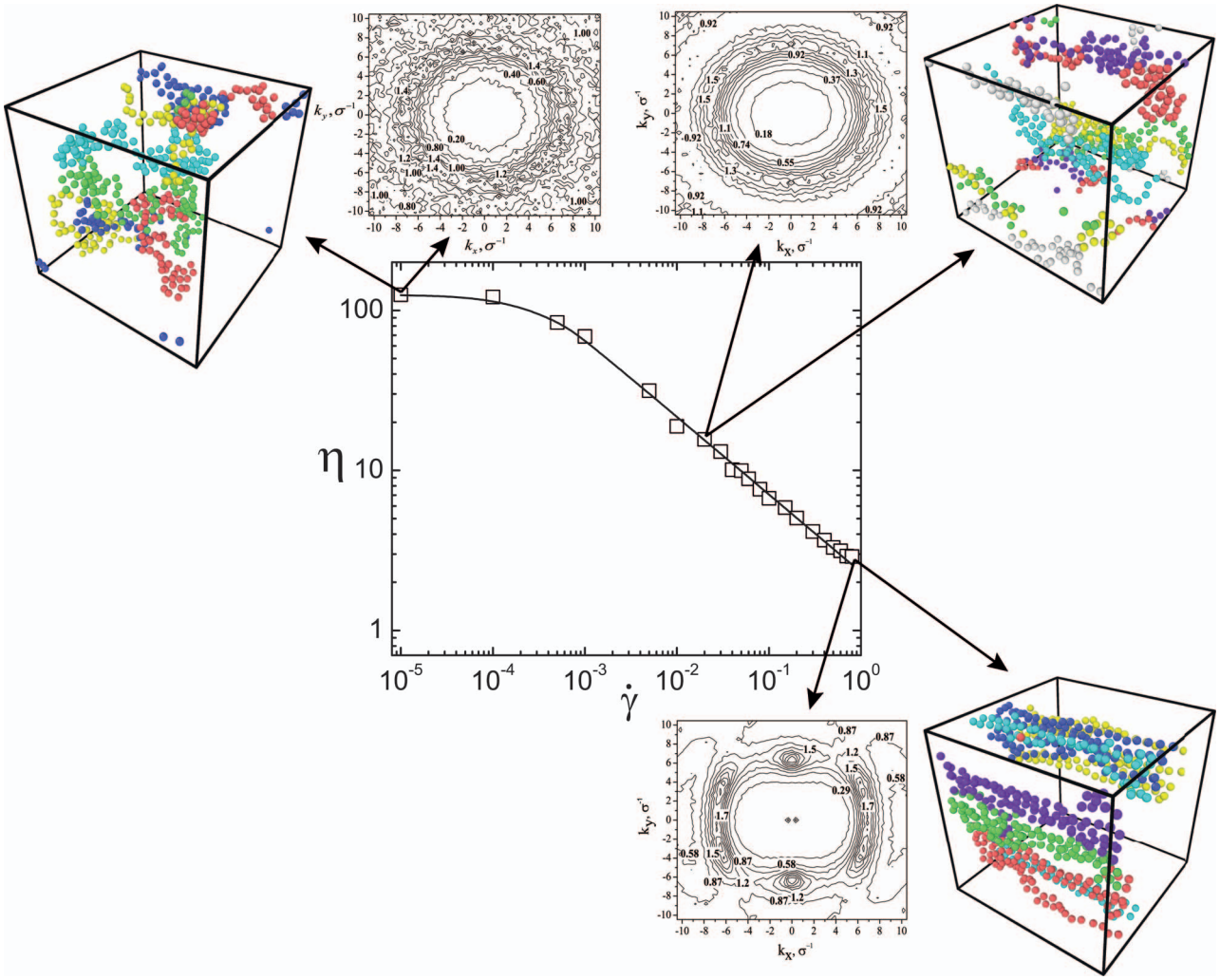

FIG. 14. Scheme to represent the relation between the static structure factor, the chain conformation, and the shear viscosity for the pure chain molecules (melt). The three-dimensional snapshots show the alignment process of the chain molecules with the flow as the shear rate increases. For the sake of clarity not all chains used in calculations are include in the three-dimensional snapshots. Note also the changes in the structure factor patterns as the shear rate increases.

conformation. As expected, the alignment of the chains causes the shear thinning.

CONCLUSIONS

In this work, NEMD simulations of linear chain solutions immersed in a Lennard-Jones solvent under simple shear flow were performed. In spite of the simplicity of the force fields employed in the simulation, the generated data reproduce, in a qualitative manner, the rheological behavior of shear-thinning fluids. Proof of this is that the calculated data of shear viscosity as a function of shear rate follow the Power-law behavior and also are well fitted to the Carreau-Yasuda model. Also, the first and second normal stress coefficients were in qualitative good agreement with simulation and experimental data of polymer solutions.

The main result of this study, however, was to establish, using molecular simulation only, the relation between the rheological properties, the static structure factor, and the molecular conformation of the chain molecules in the solutions. Particularly, it is shown that the growth of emerging peaks in the static structure factor is due to the anisotropy induced by the flow. The intensity of the dispersion, measured as the magnitude of the peaks, was also correctly calculated as being inversely proportional to the chain concentration. The ordering of the chain molecules along the flow direction is reflected in the shear thinning behavior of the fluid. The simulation results are in qualitative agreement with scattering experiments.

Finally, it was also shown that the Lennard-Jones fluid does not behave exactly as a Newtonian solvent at the shear rates considered, since it displayed some viscoelastic effects at high shear rates.

ACKNOWLEDGMENTS

The financial support of CONACYT (Project Nos. 100195, 83501, 104672, and 129962) is gratefully acknowledged.

[1]R. Bird, R. Armstrong, and O. Hassager, *Dynamics of Polymeric Liquids* (Wiley, New York, 1987).
[2]S. Saito, M. Takenaka, N. Toyoda, and T. Hashimoto, Macromolecules **34**, 6461 (2001).

[3]X.-L. Wu, D. Pine, and P. Dixon, Phys. Rev. Lett. **66**, 2408 (1991).
[4]J. van Egmond, D. Werner, and G. Fuller, J. Chem. Phys. **96**, 7742 (1992).
[5]D. Wirtz, Phys. Rev. E **50**, R1755 (1994).
[6]K. Migler, C. Liu, and D. Pine, Macromolecules **29**, 1422 (1996).
[7]J. van Egmond and G. Fuller, Macromolecules **26**, 7182 (1993).
[8]S. T. Milner, Phys. Rev. E **48**, 3674 (1993).
[9]R. G. Larson, J. Rheol. **49**, 1 (2005).
[10]C. Baig, B. J. Edwards, and D. Keffer, Rheol. Acta **46**, 1171 (2007).
[11]P. J. Daivis, M. L. Matin, and B. D. Todd, J. Non-Newtonian Fluid Mech. **147**, 35 (2007).
[12]T. C. Le, B.-D. Todd, P. J. Daivis, and A. Ulherr, J. Chem. Phys. **130**, 074901 (2009).
[13]T. C. Le, B.-D. Todd, P. J. Daivis, and A. Ulherr, J. Chem. Phys. **131**, 044902 (2009).
[14]Z. Li, H. Djohari, and E. E. Dormidontova, J. Chem. Phys. **133**, 184904 (2010).
[15]J. M. Kim, B. J. Edwards, D. J. Keffer, and B. Khomami, J. Rheol. **54**, 283 (2010).
[16]M. Kröger, W. Loose, and S. Hess, J. Rheol. **37**, 1057 (1993).
[17]J. Castillo-Tejas, J. F. J. Alvarado, G. González-Alatorre, G. Luna-Bárcenas, I. Sanchez, R. Macias-Salinas, and O. Manero, J. Chem. Phys. **123**, 054907 (2005).
[18]B. Dünweg and K. Kremer, J. Chem. Phys. **99**, 6983 (1993).
[19]T. Shimada, M. Doi, and K. Okano, J. Chem. Phys. **88**, 2815 (1988).
[20]P. Alvarez, J. Colmenero, R. Zorn, L. Willnerand, and D. Richter, Macromolecules **36**, 238 (2003).
[21]W. Burchard, A. Khalyavina, P. Linder, R. Schweins, P. Friedel, M. Wiemann, and A. Lederer, Macromolecules **45**, 3177 (2012).
[22]H. M. Laun, R. Bung, S. Hess, W. Loose, O. Hess, K. Hahn, E. Hädicke, R. Hingmann, F. Schmidt, and P. Linder, J. Rheol. **36**, 743 (1992).
[23]C. Aust, M. Kröger, and S. Hess, Macromolecules **32**, 5660 (1999).
[24]P. P. Jose and G. Szamel, J. Chem. Phys. **127**, 114905 (2007).
[25]K. Kremer and G. S. Grest, J. Chem. Phys. **92**, 5057 (1990).
[26]S. J. Plimpton, J. Comput. Phys. **117**, 1 (1995).
[27]D. J. Evans and G. P. Morris, *Statistical Mechanics of Non-equilibrium Liquids* (Academic, London, 1990).
[28]S. Nosè, Mol. Phys. **52**, 255 (1984).
[29]W. G. Hoover, Phys. Rev. A **31**, 1695 (1985).
[30]L. G. MacDowell, M. Müller, C. Vega, and K. Binder, J. Chem. Phys. **113**, 419 (2000).
[31]D. M. Heyes, Phys. Rev. B **37**, 5677 (1988).
[32]J. P. Hansen and I. McDonald, *Theory of Simple Liquids*, 3rd ed. (Elsevier, Amsterdam, 2006).
[33]M. Schoen, R. Vogelsang, and C. Hoheisel, Mol. Phys. **57**, 445 (1986).
[34]I. Teraoka, *Polymer Solutions. An Introduction to Physical Properties* (Wiley, New York, 2002).
[35]P. J. Carreau, Trans. Soc. Rheol. **16**, 99 (1972).
[36]K. Yasuda, R. C. Armstrong, and R. E. Cohen, Rheol. Acta **20**, 163 (1981).
[37]R. Larson, Rheol. Acta **31**, 497 (1992).
[38]J. T. Bosko, B. D. Todd, and R. J. Sadus, J. Chem. Phys. **121**, 12050 (2004).
[39]X. Chen, P. Carbone, W. L. Cavalcanti, G. Milano, and F. Müller-Plathe, Macromolecules **40**, 8087 (2007).
[40]M. Kontopoulou, *Applied Polymer Rheology* (Wiley, New York, 2012).
[41]W. M. Kulicke and U. Wallbaum, Chem. Eng. Sci. **40**, 961 (1985).
[42]J. Castillo-Tejas, J. F. J. Alvarado, S. Carro, F. Pérez-Villaseñor, F. Bautista, and O. Manero, J. Non-Newtonian Fluid Mech. **166**, 194 (2011).
[43]D. M. Heyes, J. Chem. Soc., Faraday Trans. 2 **82**, 1365 (1986).
[44]D. Rapaport, *The Art of Molecular Dynamics Simulation*, 2nd ed. (Cambridge University Press, New York, 2004).
[45]W. Humphrey, A. Dalke, and K. Schulten, J. Mol. Graphics **14**, 33 (1996).
[46]A. Stukowski, Modell. Simul. Mater. Sci. Eng. **18**, 015012 (2010).